INTERNATIONAL JOURNAL FOR NUMERICAL METHODS IN FLUIDS, VOL. 12, 17–41 (1991)

ON THE NUMERICAL SOLUTION OF THE TURBULENCE ENERGY EQUATIONS FOR WAVE AND TIDAL FLOWS

A. M. DAVIES AND J. E. JONES

Proudman Oceanographic Laboratory, Bidston Observatory, Birkenhead, Merseyside L43 7RA, U.K.

SUMMARY

This paper deals with the numerical solution, using finite difference methods, of the hydrodynamic and turbulence energy equations which describe wind wave and tidally induced flow.

Calculations are performed using staggered and non-staggered finite difference grids in the vertical, with various time discretizations of the production and dissipation terms in the turbulence energy equations. It is shown that the time discretization of these terms can significantly influence the stability of the solution. The effect of time filtering on the numerical stability of the solution is also considered. The form of the mixing length is shown to significantly influence the bed stress in wind wave problems.

A no-slip condition is applied at the sea bed, and the associated high-shear bottom boundary layer is resolved by transforming the equations onto a logarithmic or log–linear co-ordinate system before applying the finite difference scheme.

A computationally economic method is developed which remains stable even when a very fine vertical grid (over 200 points) is used with a time step of up to 30 min.

KEY WORDS Finite difference Hydrodynamic Turbulence energy Tidal Wind wave

1. INTRODUCTION

In a shallow homogeneous sea region, a major source of turbulence is that produced in the near-bed region, arising from flow over a rough sea bed. Currents associated with wind, tidal and wave induced motion are the primary source of this turbulence.[1–4]

In this paper we shall be concerned with the calculation of turbulence energy and current profiles produced by oscillatory motion of tidal period (of order 12 h) or wind wave period (of order 10 s). Motion at these different periods is specifically chosen to illustrate the range of bottom boundary layer thicknesses that can occur in a shallow sea and the associated numerical problems that arise in resolving them.

Analytical calculations have usually parametrized the internal shear stress in terms of a coefficient of eddy viscosity. Also, these models have in general only considered a single point in the vertical. Such models, together with near-bed observations,[5] clearly show a very-high-shear bottom boundary layer, which will have to be accurately resolved in any numerical solution of the turbulence energy equations.

Larger-scale three-dimensional hydrodynamic models of tidal flow have related the coefficient of eddy viscosity to the flow field, with eddy viscosity varying with time and horizontal position.[6,7] However, in these models the high-shear bottom boundary layer was not resolved explicitly, but rather a slip condition was applied at a height of 1 m above the bed. It is interesting to note that despite their inability to take account of the detailed physics of the near-bed region, these models

0271–2091/91/010017–25$12.50

Received February 1989
Revised January 1990

have been very successful in reproducing tidal current structure over large areas such as the Northwest European Continental Shelf. However, because these models do not resolve the near-bed region, it is not possible to use them to study the nature of near-bed turbulence.

In recent years, turbulence energy models have been used successfully to study tidal current structure at a point[8,9] and in estuaries and channels.[4,10] However, despite recent advances in computer power, application to a large-scale tidal region such as the Northwest European Shelf requires computationally accurate and efficient solution in both space and time in order to be feasible. (Similar considerations are also true of any study of wave–current interaction owing to the significantly finer horizontal grids that are required.) In this paper the first stage in the development of such a large-scale (i.e. shelf-scale) turbulence energy model, namely the investigation of the accuracy and stability of various finite difference solutions, is considered. Here we present a number of numerical methods that can be used to solve the turbulence energy equations for wave and tidally induced motion at a point.

Section 2 of this paper describes the turbulence energy equations and various forms of the mixing length. In Section 3 various numerical methods are presented for the solution of these equations, and in Section 4 the numerical stability and accuracy of the solutions for both wave and tidally induced currents are examined in some detail.

Some discussion of the influence of mixing length upon current profiles, viscosity profiles and, in particular, bed stress, together with a detailed assessment of the stability and accuracy of various difference schemes, is presented in the latter part of the paper.

In essence the paper reviews and compares and contrasts different methods of solving the turbulence energy equations for two different geophysical flow regimes, namely tides and wind waves.

2. MODEL EQUATIONS

The linear hydrodynamic equations at a point can be written as

$$\frac{\partial u}{\partial t} - fv = \frac{\partial P}{\partial x} + \frac{\partial}{\partial z}\left(\mu \frac{\partial u}{\partial z}\right), \tag{1}$$

$$\frac{\partial v}{\partial t} + fu = \frac{\partial P}{\partial y} + \frac{\partial}{\partial z}\left(\mu \frac{\partial v}{\partial z}\right). \tag{2}$$

In these equations, u and v are the x- and y-components of current in a Cartesian co-ordinate system, with z, the vertical co-ordinate, having its origin at the sea bed and increasing upwards. The Coriolis parameter f is constant and μ denotes the coefficient of vertical eddy viscosity, with P the externally specified pressure forcing.

For sinusoidally induced pressure forcing at a point, it is convenient to express $\partial P/\partial x$ and $\partial P/\partial y$ as

$$\frac{\partial P}{\partial x} = h_x \omega \cos(\omega t), \tag{3}$$

$$\frac{\partial P}{\partial y} = h_y \omega \cos(\omega t) \tag{4}$$

with h_x and h_y denoting the amplitude of the external forcing and ω its period.

A no-slip boundary condition is applied at the sea bed; thus

$$u = 0 \quad \text{and} \quad v = 0 \quad \text{at} \quad z = z_0, \tag{5}$$

with z_0 the roughness length.

For wave and tidally induced flows, at the sea surface $z=h$ (with h the water depth) a zero-stress condition is applied; thus

$$\mu \left.\frac{\partial u}{\partial z}\right|_{z=h} = 0, \qquad \mu \left.\frac{\partial v}{\partial z}\right|_{z=h} = 0. \tag{6}$$

We now consider the calculation of the eddy viscosity μ in terms of a mixing length l and turbulence energy b determined from

$$\frac{\partial b}{\partial t} = \mu\left[\left(\frac{\partial u}{\partial z}\right)^2 + \left(\frac{\partial v}{\partial z}\right)^2\right] + \beta \frac{\partial}{\partial z}\left(\mu \frac{\partial b}{\partial z}\right) - \varepsilon, \tag{7}$$

with the turbulence dissipation ε computed from

$$\varepsilon = C_1 b^{3/2}/l \tag{8}$$

and the eddy viscosity given by

$$\mu = C_0 l b^{1/2}. \tag{9}$$

Values of the coefficients β, C_0 and C_1 have been given by Vager and Kagan[8] as $\beta = 0{\cdot}73$, $C_0 = C^{1/4}$ and $C_1 = C_0^3$, where $C = 0{\cdot}046$. Mofjeld and Lavelle,[9] however, take $C_0 = (15)^{-1/3}$. Although there are some slight differences in these coefficients, King *et al.*[2] found that they made little difference to the levels of turbulence and current profiles induced by tidal or wave forcing.

Various algebraic expressions for the mixing length are presented in the literature and a number of them are considered here.

The simplest form of the mixing length is one in which it increases linearly with height above the sea bed; thus

$$l = K(z_0 + z), \tag{10}$$

with $K = 0{\cdot}4$ being Von Karman's constant.

Vager and Kagan[8] give an expression for l which on integration[10,11] gives

$$l = K b^{1/2}\left(\int_{z_0}^{z} b^{-1/2}\,\mathrm{d}z + z_0 b_0^{-1/2}\right), \tag{11}$$

with b_0 denoting the turbulence energy at the sea bed. It is evident that (11), unlike the earlier expression (10), yields a mixing length that depends upon the turbulence energy intensity in the water column. An alternative expression, also depending upon turbulence energy, was proposed by Blackadar,[12] of the form

$$l = \frac{Kz}{1 + Kz/l_0}, \tag{12}$$

with

$$l_0 = \gamma \int_{z_0}^{h} b^{1/2} z\,\mathrm{d}z \Big/ \int_{z_0}^{h} b^{1/2}\,\mathrm{d}z, \tag{13}$$

where γ is a constant in the range 0·1–0·4.

For wave and tidally induced flows, appropriate sea surface and sea bed boundary conditions for turbulence energy are

$$\left.\frac{\mathrm{d}b}{\mathrm{d}z}\right|_{z=h} = 0, \qquad \left.\frac{\mathrm{d}b}{\mathrm{d}z}\right|_{z=z_0} = 0. \tag{14}$$

Besides the calculation of the velocity, turbulence energy, viscosity and mixing length fields, it is also instructive to calculate stress profiles τ_x and τ_y from

$$\tau_x = \rho\mu \frac{\partial u}{\partial z}, \qquad \tau_y = \rho\mu \frac{\partial v}{\partial z}. \tag{15}$$

As we shall show later, this profile reaches a maximum in the near-bed region. In circumstances where the finite difference grid used to solve these equations (see Section 3) or the time step used to integrate them is not sufficiently fine, the bottom stress exhibits time step oscillations, which prove to be an early indicator of when instabilities will corrupt the total solution.

An alternative means of computing the modulus of the bed stress is from

$$|\tau| = \rho C^{1/2} b_0, \tag{16}$$

with b_0 the turbulence intensity at the bed.

Equation (16) can be readily derived from the steady state form of (7) if turbulent diffusion is neglected. It is important to note that these assumptions imply that turbulence production and dissipation balance, which is not always true. It is, however, interesting to compare the modulus of bed stress derived from (15) with that determined from (16), and some examples are given in Section 4.

3. NUMERICAL SOLUTION OF THE HYDRODYNAMIC AND TURBULENCE EQUATIONS

Here we consider the solution of the time-dependent equations (1), (2) and (7) using staggered and non-staggered grids in the vertical (see Figure 1, grids A and B). In grid A, vertical differencing of the current (i.e. current shear) gives the turbulence production term at the turbulence point.

3.1. Transformation of equations

Before developing the finite difference solution of these equations, we will briefly consider their transformation onto a logarithmic or log–linear co-ordinate system using:

logarithmic transform

$$\sigma = \ln (z/z_0)/\alpha, \tag{17}$$

with

$$\alpha = \ln (z/h); \tag{18}$$

log–linear transform

$$\sigma = \ln (z/z_0) + [(z - z_0)/z_*]/\alpha, \tag{19}$$

with

$$\alpha = \ln (h/z_0) + (h - z_0)/z_*. \tag{20}$$

In (20), z_* is an arbitrary height parameter which can be used to determine the height above the sea bed over which the grid is essentially logarithmic.

It can be readily shown from (17) and (18) that

$$\frac{\partial}{\partial z} = \frac{1}{\chi} \frac{\partial}{\partial \sigma}, \tag{21}$$

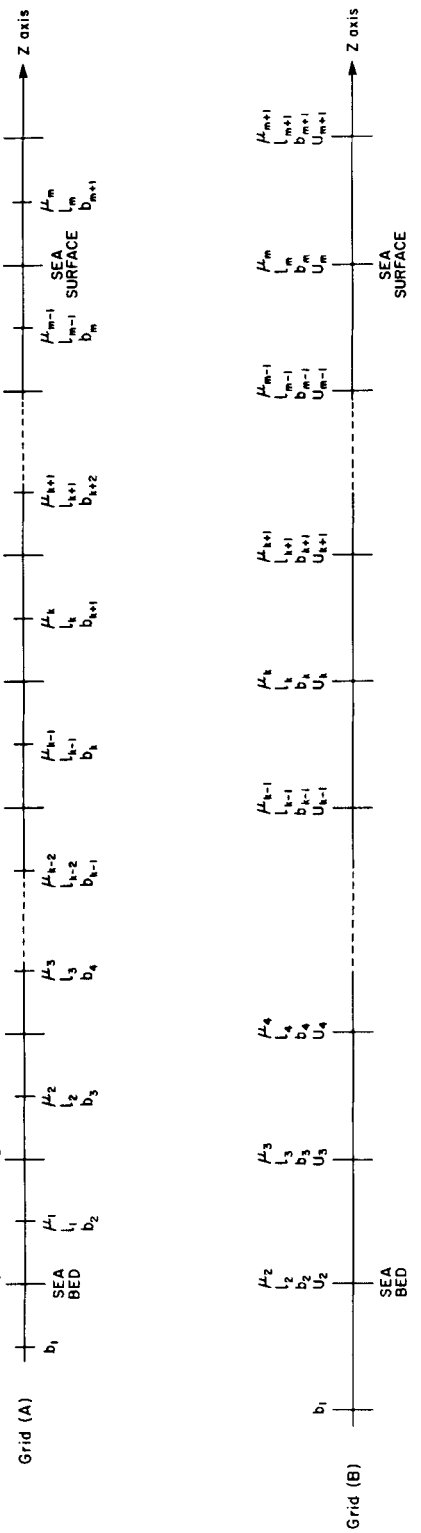

Figure 1. Staggered (grid A) and non-staggered (grid B) finite difference grids in the vertical

with

$$\chi = z_0 \alpha e^{\alpha\sigma}. \tag{22}$$

Using equation (1) for illustrative purposes, it is evident that substituting (21) into (1) gives the transformed equation

$$\frac{\partial u}{\partial t} - fv = \frac{\partial P}{\partial x} + \frac{1}{\chi}\frac{\partial}{\partial \sigma}\left(\frac{\mu}{\chi}\frac{\partial u}{\partial \sigma}\right). \tag{23}$$

An alternative suggested by King *et al.*[2] is to integrate the term involving μ by parts and then apply the transformation; thus

$$\frac{\partial u}{\partial t} - fv = \frac{\partial P}{\partial x} + \frac{\mu}{\chi^2}\frac{\partial^2 u}{\partial \sigma^2} + \frac{1}{\chi^2}\left(\frac{\partial \mu}{\partial \sigma} - \mu\omega\right)\frac{\partial u}{\partial \sigma}, \tag{24}$$

with $\omega = \alpha$ in the case of a logarithmic transformation.

Similarly, transforming (7) gives

$$\frac{\partial b}{\partial t} = \frac{\mu}{\chi^2}\left[\left(\frac{\partial u}{\partial \sigma}\right)^2 + \left(\frac{\partial v}{\partial \sigma}\right)^2\right] + \frac{\beta}{\chi}\frac{\partial}{\partial \sigma}\left(\frac{\mu}{\chi}\frac{\partial b}{\partial \sigma}\right) - \varepsilon. \tag{25}$$

Integrating μ by parts then applying the transformation gives

$$\frac{\partial b}{\partial t} = \frac{\mu}{\chi^2}\left[\left(\frac{\partial u}{\partial \sigma}\right)^2 + \left(\frac{\partial v}{\partial \sigma}\right)^2\right] + \beta\frac{\mu}{\chi^2}\frac{\partial^2 b}{\partial \sigma^2} + \frac{\beta}{\chi^2}\left(\frac{\partial \mu}{\partial \sigma} - \mu\omega\right)\frac{\partial b}{\partial \sigma} - \varepsilon. \tag{26}$$

The transformation of the various mixing length equations given in Section 2 proceeds in an analogous manner, and details will not be given here.

3.2. *Finite difference solution (staggered grid)*

Consider initially the solution of equation (23) using a Crank–Nicolson-like method in the time domain and the staggered grid (Figure 1, grid A) in the vertical.

Thus at the kth grid point

$$(U_k^{t+\tau} - U_k^t)/\tau - f V_k^t = \frac{\partial P^{t+\theta_1\tau}}{\partial x} + \frac{\theta_1 W_k}{\Delta^2}(\mu_k^t \bar{W}_k \delta U_k^{t+\tau} - \mu_{k-1}^t \bar{W}_{k-1}\delta U_{k-1}^{t+\tau}) + \frac{\theta_2 W_k}{\Delta^2}(\mu_k^t \bar{W}_k \delta U_k^t - \mu_{k-1}^t \bar{W}_{k-1}\delta U_{k-1}^t), \tag{27}$$

with $\delta U_k = U_{k+1} - U_k$ and Δ the vertical grid spacing. Also $W_k = 1/\chi$ evaluated at U grid point k and $\bar{W}_k = 1/\chi$ evaluated at the midpoint between U grid points $k+1$ and k (see Figure 1, grid A), with τ the time step.

In equation (27) the time-weighting term θ_1 lies in the range $0 \leqslant \theta_1 \leqslant 1$, with $\theta_2 = 1 - \theta_1$.

The sea bed boundary condition is incorporated in (27) by defining $U_1 = 0$. The inclusion of the sea surface condition is accomplished by setting $U_m = U_{m-1}$.

In the explicit case ($\theta_1 = 0$) a stability analysis based upon a grid resolution of order 0·005 m in the near-bed region (necessary in order to adequately resolve the high-shear layer) required a time step of order 0·0025 s for a typical μ of 0·01 $m^2 s^{-1}$—clearly impractical.

In the case in which θ_1 is non-zero, an implicit solution ($\theta_1 = 1{\cdot}0$) or a semi-implicit solution ($\theta_1 = 0{\cdot}5$) is obtained, which on a regular grid can be shown to be unconditionally stable. The application of an implicit or a semi-implicit method, with the grid-differencing given above, leads

to the solution of a set of simultaneous equations involving a tridiagonal matrix. Details of the form of the matrix equations and solution using the Thomas method are standard and can be found in Reference 13.

Consider the solution of (25):

$$\frac{b_k^{t+\tau}-b_k^t}{\tau}=\mu_{k-1}\frac{\bar{W}_{k-1}^2}{\Delta^2}[(\gamma_1\delta U_{k-1}^{t+\tau}+\gamma_2\delta U_{k-1}^t)^2+(\gamma_1\delta V_{k-1}^{t+\tau}+\gamma_2\delta V_{k-1}^t)^2]$$
$$+\theta_1\frac{\beta\bar{W}_{k-1}}{\Delta^2}\left(W_k\frac{\mu_k^t+\mu_{k-1}^t}{2}\delta b_k^{t+\tau}-W_{k-1}\frac{\mu_{k-1}^t+\mu_{k-2}^t}{2}\delta b_k^{t+\tau}\right)$$
$$+\theta_2\frac{\beta\bar{W}_{k-1}}{\Delta^2}\left(W_k\frac{\mu_k^t+\mu_{k-1}^t}{2}\delta b_k^t-W_{k-1}\frac{\mu_{k-1}^t+\mu_{k-2}^t}{2}\delta b_k^t\right)-\varepsilon. \tag{28}$$

Again in this equation the coefficients θ_1 and θ_2 can be used to time-centre the term describing the diffusion of turbulent energy. The coefficients γ_1 and γ_2 are such that $\gamma_2=1-\gamma_1$, with γ_1 lying in the range $0\leqslant\gamma_1\leqslant 1$. The choice of these coefficients determines the degree of centring of the turbulence production term. An alternative finite difference form of this equation is described in the Appendix.

Consider now the temporal form of the dissipation term in (7). Using (8), one possible form, which places some of the dissipation at the higher time step, is

dissipation A

$$\varepsilon=C_1 b_k^{t+\tau}(b_k^t)^{1/2}/l_{k-1}^t. \tag{29}$$

Alternatively, eliminating l from (8), using (9) and time-centring b gives a fully time-centred form

dissipation B

$$\varepsilon=C_1 C_0 b_k^{t+\tau}b_k^t/\mu_{k-1}^t. \tag{30}$$

A less obvious time distribution of b, which we shall show later to have good stability properties, is to express ε as

dissipation C

$$\varepsilon=C_1 C_0[2b_k^{t+\tau}b_k^t-(b_k^t)^2]/\mu_{k-1}^t. \tag{31}$$

Surface and bed boundary conditions (14) can be readily accomplished using

$$b_1=b_2 \quad \text{(bed boundary)}, \qquad b_{m+1}=b_m \quad \text{(surface boundary)}.$$

Solving these equations using an implicit ($\theta_1=1$) or a semi-implicit ($\theta_1=0{\cdot}5$) time-differencing scheme again yields a tridiagonal matrix problem which is solved in an identical manner to that described above.

Calculation of the mixing length using expressions (10)–(13) does not involve a time-stepping problem. In the case in which the mixing length depends upon the turbulence energy, its value at the new time step was determined from the turbulence energy at this time step, computed by solving (28) prior to determining the mixing length.

Calculation of the eddy viscosity μ at the higher time step was accomplished using (9) with l and b at this higher time step.

By solving the equations in this order, the velocity field, turbulence energy, mixing length and eddy viscosity can be advanced through time. In this sequence of solutions the eddy viscosity μ in equations (27) and (28) is taken at the lower time step. The eddy viscosity in these equations could

be included at a higher time step by essentially a multistep predictor–corrector procedure in which (27) and (28) were first solved with μ at the lower time step and were then re-solved with μ at the higher time step. Obviously the determination of μ at the higher time step requires the solution of the turbulence energy and mixing length equations, with the associated computer overhead. In practice this sequence of operations could be performed a number of times until the final μ- and l-values at the higher time step were essentially unchanged. However, as is to be expected, this iterative sequence of operations is computationally time-consuming, but was found to enhance the stability of the solution in some cases (a point discussed in detail in the next sub-section).

The effect upon stability and accuracy of introducing some time filtering every n time steps was also examined (Section 4) using a simple Schuman[14] time filter of the form

$$\bar{F}(t)=F(t)+0{\cdot}5v[F(t+\tau)-2F(t)+F(t-\tau)], \tag{32}$$

or the slightly more selective though computationally more expensive filter of Asselin,[15] given by

$$\bar{F}(t)=F(t)+0{\cdot}5v[F(t+\tau)-2F(t)+\bar{F}(t-\tau)]. \tag{33}$$

In these equations $\bar{F}(t)$ is the new filtered value (current or turbulence energy) at the time step t, and v, in the range $0\leqslant v\leqslant 1$, is the weighting which determines the extent of the filtering. In the cases considered later, $v=0{\cdot}5$, giving the conventional 'one–two–one' filter from equation (32). Obviously, as is well known,[16] if these filters are applied at frequent intervals (low n-values), they can damp the long waves. Also, since each application of the filter requires an additional forward time step to compute $F(t+\tau)$ and further calculations to compute $\bar{F}(t-\tau)$ for the Asselin[15] filter, frequent filtering can be computationally expensive.

3.3. *Finite difference solution (non-staggered grid)*

Here we briefly describe the solution of the equations using a non-staggered grid in the vertical (Figure 1, grid B) with the Crank–Nicolson time-differencing method. By way of contrast with the previous subsection, here we use the form of the equations in which the viscosity term has been differentiated by parts, namely equations (24) and (26).

Considering initially the u-equation of motion (24), at the kth grid point we have

$$\begin{aligned}(U_k^{t+\tau}-U_k^t)/\tau - f V_k^t = {} & \frac{\partial P^{t+\theta_1\tau}}{\partial x}+\frac{\theta_1 W_k\mu_k}{\Delta^2}(U_{k+1}^{t+\tau}-2U_k^{t+\tau}+U_{k-1}^{t+\tau})+\theta_1 W_k\left[\left(\frac{\mu_{k+1}^t-\mu_{k-1}^t}{2\Delta}\right)-\mu_k^t\omega_k\right]\\ & \times\left(\frac{U_{k+1}^{t+\tau}-U_{k-1}^{t+\tau}}{2\Delta}\right)+\frac{\theta_2 W_k\mu_k}{\Delta^2}(U_{k+1}^t-2U_k^t+U_{k-1}^t)\\ & +\theta_2 W_k\left[\left(\frac{\mu_{k+1}^t-\mu_{k-1}^t}{2\Delta}\right)-\mu_k^t\omega_k\right]\left(\frac{U_{k+1}^t-U_{k-1}^t}{2\Delta}\right),\end{aligned} \tag{34}$$

with ω_k the value of α ((see equations (18) or (20)) at the kth grid box.

The sea bed boundary condition is incorporated into (34) by setting $U_2=0$ (see Figure 1, grid B) and the sea surface by setting $U_{m+1}=U_m$.

Considering the solution of (26), using grid (B) and the Crank–Nicolson method gives

$$\begin{aligned}\frac{b_k^{t+\tau}-b_k^t}{\tau} = {} & \frac{\mu_k W_k^2}{2\Delta}[(\gamma_1\bar{\delta}U_k^{t+\tau}+\gamma_2\bar{\delta}U_k^t)^2+(\gamma_1\bar{\delta}V_k^{t+\tau}+\gamma_2\bar{\delta}V_k^t)^2]\\ & +\theta_1\beta\frac{\mu_k W_k}{\Delta^2}(b_{k+1}^{t+\tau}-2b_k^{t+\tau}+b_{k-1}^{t+\tau})+\frac{\theta_1\beta W_k}{2\Delta}\end{aligned}$$

$$\times\left(\frac{\bar{\delta}U_k}{2\Delta}-\mu_k\omega_k\right)\bar{\delta}b_k^{t+\tau}+\theta_2\beta\frac{\mu_k W_k}{\Delta^2}(b_{k+1}^t-2b_k^t+b_{k-1}^t)$$

$$+\theta_2\frac{\beta W_k}{2\Delta}\left(\frac{\bar{\delta}U_k}{2\Delta}-\mu_k\omega_k\right)\bar{\delta}b_k^t-\varepsilon. \tag{35}$$

Here the same finite difference form of the production term has been used as in (28) for stability reasons; alternatives are possible (see Appendix) but are less stable.

In (35) the operator $\bar{\delta}$ is the central difference operation; thus, for example, $\bar{\delta}U_k=U_{k+1}-U_{k-1}$. In an analogous manner to that employed with the staggered grid, we consider three different forms of the dissipation term, namely

dissipation A

$$\varepsilon=C_1 b_k^{t+\tau}(b_k^t)^{1/2}/l_k^t, \tag{36}$$

dissipation B

$$\varepsilon=C_1 C_0 b_k^{t+\tau} b_k^t/\mu_k^t, \tag{37}$$

dissipation C

$$\varepsilon=C_1 C_0[2b_k^{t+\tau}b_k^t-(b_k^t)^2]/\mu_k^t. \tag{38}$$

Surface and bed boundary conditions can be approximated by

$$b_1=b_2 \quad \text{(bed boundary)}, \qquad b_{m+1}=b_m \quad \text{(surface boundary)}.$$

It is important to note that on the non-staggered grid, unlike the staggered grid, application of this boundary condition implies that $\partial b/\partial z=0$ at $0{\cdot}5\Delta$ above the sea surface and a similar distance below the sea bed. However, $\partial b/\partial z$ can be set to zero on these boundaries by using

$$b_1=b_3, \qquad b_{m+1}=b_{m-1}.$$

Calculation of the mixing length and eddy viscosity is accomplished in a similar manner to that employed with the staggered grid, using values of b for the mixing length, and b and l for the eddy viscosity at the higher time step. Iteration to give consistent values of μ is also possible but computationally expensive.

4. CALCULATION OF WAVE AND TIDALLY INDUCED CURRENTS

In this section the turbulence energy model described in Section 3, with various formulations of the mixing length, is used to calculate the wave or tidally induced current, turbulence energy and eddy viscosity. These calculations are used to examine whether there is any significant advantage in using a staggered rather than a non-staggered grid. The effect upon numerical stability of the various formulations (namely A, B or C) of the dissipation term (equations (29)–(31) or (36)–(38)) is also considered. The various forms of the production term (see Appendix) are briefly examined. The influence upon the accuracy of the final solution of refining the vertical grid by increasing the number of grid boxes, m, over the range 25, 50, 100 and 200 using both logarithmic and log–linear transformed grids is examined in some detail. In all calculations the bed roughness z_0 was fixed at 0.005 m (a typical shallow sea value[3]) but the water depth h was varied.

4.1. Wave induced flow, water depth $h = 10$ m, wave period $T = 8\ s^{-1}$

In this calculation, motion was induced by an oscillating forcing in the x-direction, of unit amplitude ($h_x = 1{\cdot}0$ m s^{-1}, $h_y = 0{\cdot}0$ in (3) and (4)) and period 8 s^{-1} (a typical wind wave period). The Coriolis term f was zero. It is evident from Figure 2(a) that for such a high-frequency wave the bottom boundary layer is of order 0·20 m thick and consequently occupies only a small part of the water column. Above this bottom boundary a free stream flow (no variation of current in the vertical) is present in which the stress is zero (Figure 2(b)). Obviously a grid transformation giving the maximum number of grid points within the high-shear bottom layer (the logarithmic transformation) will be optimal for the problem of the wave alone. However, in a physically more realistic situation in which, waves, currents and wind induced turbulence would be considered in combination, a grid with significant resolution above the bottom layer would be required. (This is particularly so for wind induced flow, where a turbulent surface layer exists.[17] Also, examples of tidal flow requiring adequate grid resolution in the upper part of the water column will be presented later.) For this reason and also for computational economy it is important to examine the accuracy of the solution for vertical grids of various resolutions (i.e. a range of m-values) and different transformations.

In an initial series of calculations a time step τ of 0.05 s was employed. Since the method is implicit, in theory stability is assured for any time step. Such a small time step was used so that time discretization errors would not influence the solution. The calculation was started from a state of zero velocity, although the eddy viscosity μ, turbulence energy b and mixing length l were assigned small initial values, namely $\mu = 1{\cdot}0 \times 10^{-6}$ m^2 s^{-1}, $b = 1{\cdot}0 \times 10^{-6}$ m^2 s^{-2} and $l = 1{\cdot}0 \times 10^{-6}$ m, in order to avoid division by zero in the turbulence equations (see Section 2) and the possibility of negative turbulence energy in the first few time steps. After five or six wave periods (time $T = 48$ s for an 8 s wave) the effect of the initial conditions had been removed. However, the solution was integrated up to 120 s before being harmonically analysed to ensure the complete removal of any transients. Values of the amplitude of the fundamental harmonic of the current at various heights above the bed, together with instantaneous values of stress, viscosity, turbulence energy and mixing length at time $T = 1560\tau$ ($\tau = 0{\cdot}05$ s), are given in Table I. Also shown in the table are values of the maximum bed stress over a wave cycle computed using either (a) the vertical derivative of the current at the bed (equation (15)) or (b) the turbulent energy (equation (16)). These bed stress values computed with the mixing length of Vager and Kagan[8] are in excellent agreement with recently published[3] independent calculations.

Table I shows the influence of reducing the grid resolution from $m = 200$ grid boxes to $m = 100$ and finally $m = 25$ grid boxes. The mixing length formulation of Vager and Kagan[8] ((equation (11)) was used in this calculation. From this table it is evident that reducing m from 200 to 100 and changing from a logarithmic transform (the optimum one for this problem) to a log–linear transform ($z_* = 0{\cdot}5$ in sigma co-ordinates) did not significantly influence the solution (compare the first two sets of values in Table I). A further reduction in the number of grid boxes to $m = 25$ does have some effect upon the accuracy of the solution, especially the value of the mixing length at a height of 0·1 (see Table I) above the bed. This is to be expected since the mixing length depends upon the integral of the turbulence up to a given height, and as the grid resolution is reduced, accuracy will also diminish.

Computed values determined using the staggered grid (Figure 1, grid A) in the vertical are also shown in the table. These were not significantly different from those computed using the non-staggered grid. This is particularly important since it confirms that the solution is independent of the finite difference method used and suggests, together with the previous results, that an accurate solution has been obtained.

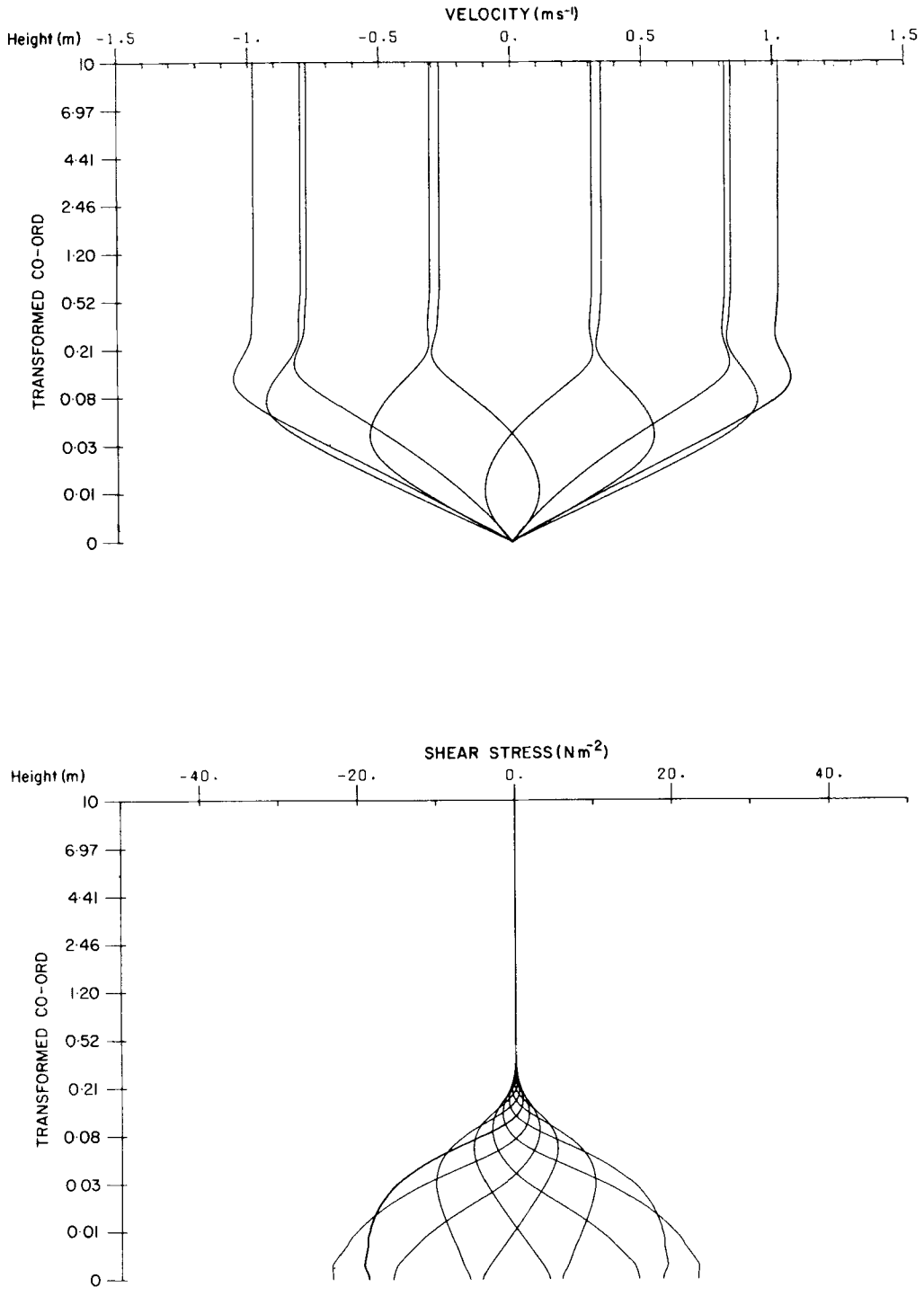

Figure 2. Profiles over a wave period on a transformed co-ordinate of (a) current velocity and (b) shear stress computed for a wave of period $T=8$ s in a water depth $h=10$ m using the mixing length formulation of Blackadar with $\gamma=0{\cdot}4$

Table I. Influence of grid resolution upon wave results computed using the mixing length of Vager and Kagan.[8] Instantaneous values are at a time 1560τ ($\tau = 0{\cdot}05$ s) from the start of the calculation

$s=z/h$-co-ord.	$h(\mathrm{m\,s^{-1}})\times 10^2$	$\tau(\mathrm{N\,m^{-2}})$	$\mu(\mathrm{m^2\,s^{-1}})\times 10^4$	$b(\mathrm{m\,s^{-1}})\times 10^2$	$l(\mathrm{m})\times 10^2$	Max. bed stress ($\mathrm{N\,m^{-2}}$)
$m=200$, non-staggered logarithmic grid						
0·001	28·78	20·09	5·54	9·11	0·40	(a) 23·95
0·0025	65·19	18·22	12·18	7·79	0·94	(b) 22·32
0·1	100·00	0·01	10·70	0·03	14·43	
$m=100$, non-staggered log–linear grid						
0·001	28·19	19·81	5·47	9·10	0·39	(a) 23·21
0·0025	65·09	18·19	12·16	7·79	0·94	(b) 22·24
0·1	100·00	0·01	8·54	0·02	12·80	
$m=25$, non-staggered log–linear grid						
0·001	28·18	19·95	5·50	9·03	0·39	(a) 22·97
0·0025	65·57	18·29	12·26	7·82	0·95	(b) 22·19
0·1	100·00	0·00	2·94	0·01	5·48	
$m=100$, staggered log–linear grid						
0·001	28·64	20·09	5·79	9·15	0·41	(a) 23·94
0·0025	65·09	18·05	12·62	7·92	0·98	(b) 22·29
0·1	100·00	0·01	9·56	0·04	14·12	

Values of the parameters shown in the table were also computed with a fixed mixing length, one increasing linearly with height above the bed (equation (10)) and that given by Blackadar[12] with $\gamma = 0{\cdot}4$. These calculations did not show a significant difference between the results computed with this mixing length, that of Vager and Kagan, and that of Blackadar with $\gamma = 0{\cdot}4$ (see Table II). However, solutions computed with Blackadar's mixing length with $\gamma = 0{\cdot}1$ were significantly different from those determined previously (see Table II). It is evident that with $\gamma = 0{\cdot}1$ the stress, viscosity and mixing length are significantly reduced below those obtained previously (compare Tables I and II, and Figures 2 and 3). It is evident from a comparison of Figures 2(b) and 3 that reducing γ from 0·4 to 0·1 reduces the magnitude of the bed stress and the thickness of the wave boundary layer. However, the increase in boundary layer thickness with increasing γ is important numerically in that the region of higher grid resolution should be larger if the boundary layer is larger.

Since the form of the mixing length given by Blackadar[12] is significantly different from that of Vager and Kagan,[8] it can be used as another check of the independence of the solution from the grid (i.e. whether a non-staggered or staggered grid is employed). It is evident from Table II with $m = 100$ that there is no significant difference in the results computed using either the staggered or non-staggered grid. Consequently, the difference in solutions between those computed with $\gamma = 0{\cdot}4$ and 0·1 is physically realistic and of some importance. The difference in bed stress is particularly important in any problem where the magnitude of the bed stress is crucial, e.g. sediment transport problems.

In these calculations a time step of 0·05 s was used with turbulence production given by equation (41) (see later for a discussion of this). No significant difference (see Table III) between the solutions computed using the various dissipation formulations (A, B or C) was obtained. (In fact, A

Table II. Influence of the parameter γ in the mixing length formulation of Blackadar[12] upon computed properties of the wind wave. Instantaneous values are at a time 1560τ ($\tau = 0{\cdot}05$ s) from the start of the calculation

$s=z/h$-co-ord.	$h(\mathrm{m\ s^{-1}}) \times 10^2$	$\tau(\mathrm{N\ m^{-2}})$	$\mu(\mathrm{m^2\ s^{-1}}) \times 10^4$	$b(\mathrm{m\ s^{-1}}) \times 10^2$	$l(\mathrm{m}) \times 10^2$	Max. bed stress ($\mathrm{N\ m^{-2}}$)
$m=100$, $\gamma=0{\cdot}4$, non-staggered log–linear grid						
0·001	29·07	18·85	5·14	11·25	0·38	(a) 23·31
0·0025	66·47	16·76	10·89	9·49	0·87	(b) 21·78
0·10	100·00	0·00	9·81	0·00	5·79	
$m=100$, $\gamma=0{\cdot}1$, non-staggered log–linear grid						
0·001	35·62	6·63	1·35	4·11	0·16	(a) 10·70
0·0025	91·28	3·49	1·26	2·06	0·21	(b) 9·88
0·10	100·00	0·00	0·00	0·00	0·27	
$m=100$, $\gamma=0{\cdot}1$, staggered log–linear grid						
0·001	36·14	6·74	1·40	4·20	0·17	(a) 10·94
0·0025	90·67	3·33	1·28	2·32	0·23	(b) 9·93
0·10	100·00	0·00	0·00	0·00	0·28	

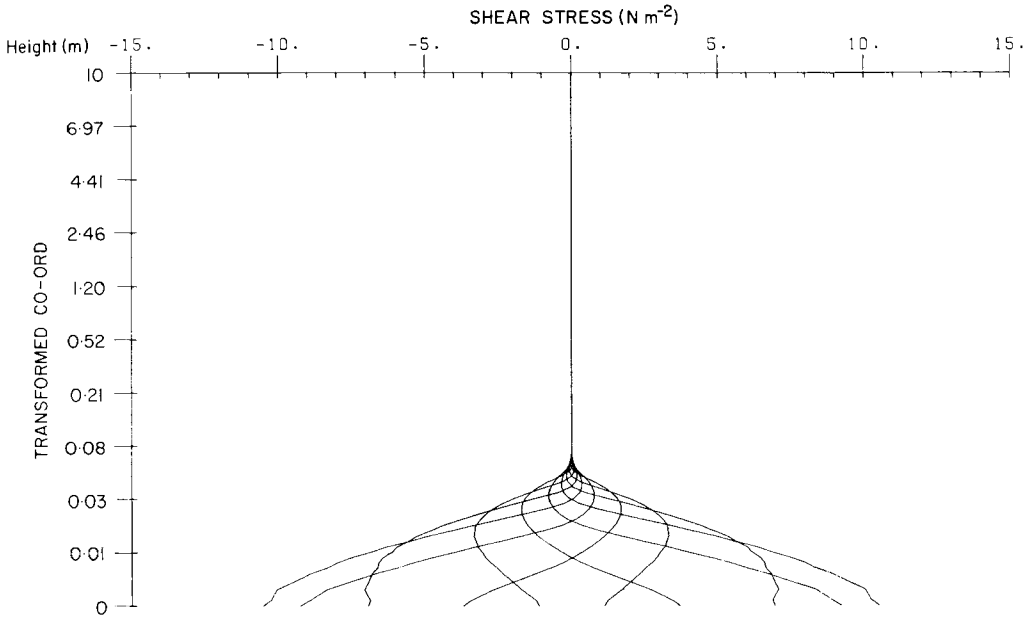

Figure 3. As for Figure 2(b) but with $\gamma = 0{\cdot}1$

Table III. Influence of time step τ and finite difference form of turbulence dissipation upon numerical stability. Values shown in the table are maximum bed stress (τ) and amplitude of the fundamental harmonic for a wave of 8 s period in a water depth $h = 10$ m. The mixing length of Vager and Kagan[8] was used in the calculation

				Vertical co-ordinate $s = z/h$	
		(a)	(b)	$s = 0{\cdot}001$	$s = 0{\cdot}01$
Diss.	τ(s)	τ(N m^{-2})	τ(N m^{-2})	U(m s^{-1}) $\times 10^2$	U(m s^{-1}) $\times 10^2$
A	0·05	23·31	22·38	28·15	103·9
B		23·31	22·38	28·15	103·9
C		23·21	22·24	28·19	104·0
A	0·20	23·39	22·38	28·45	104·5
B		23·39	22·38	28·45	104·5
C		22·95	21·71	28·61	104·8
A	0·40	26·18 *	22·81 *	28·80	105·5
B		26·18 *	22·81*	28·80	105·5
C		22·20	20·99	29·08	105·9

* Indicates that the computed solution exhibited time step oscillations in the bottom stress.
(a) Bed stress computed using equation (15); (b) computed using equation (16).

and B gave identical solutions.) However, in any longer-period calculation it would be computationally economical to use as long a time step as possible, and for this reason a range of calculations were performed with τ taking values 0·2 and 0·4 s, again with each form of the dissipation term (Table III).

It is apparent from Table III that using a time step $\tau = 0{\cdot}2$ s with dissipation from A, B or C yielded a solution which was only slightly different (a difference of less than 2%) from that obtained with $\tau = 0{\cdot}05$ s. However, when the time step was increased to $\tau = 0{\cdot}4$ s the bed stress computed using vertical differencing (equation (15)) with dissipation forms A and B showed a slight time step oscillation in the bed stress (of order 5% of the bed stress). This oscillation was not found in the solution using dissipation form C. However, in all cases the bed stress computed with $\tau = 0{\cdot}4$ s (although not the currents) was significantly different from that computed with $\tau = 0{\cdot}05$ s. This difference and the presence of time step oscillations in the bed stress suggest that the use of such a large time step ($\tau = 0{\cdot}4$ s) gives physically unacceptable solutions. However, dissipation forms A, B and C appeared equally acceptable in the wave problem. We will, however, show that this is not true for tidally induced turbulence.

4.2. Tidally induced flow, water depth = 10 m, wave of M_2 tidal period ($T = 12{\cdot}42$ h)

It is evident from the previous calculation that for wind waves having a period of 8 s^{-1} the bottom boundary layer has a thickness of order 0·20 m. However, for much-longer-period waves (e.g. tidal waves) a significantly thicker boundary layer occurs, which in shallow water can occupy the whole water column (see Figure 4(a)). In tidal problems the influence of rotation cannot be neglected as in the case of wind waves. However, in an initial series of calculations we will consider a rectilinear tidal flow, which might occur in a narrow channel, and neglect the influence of rotation.

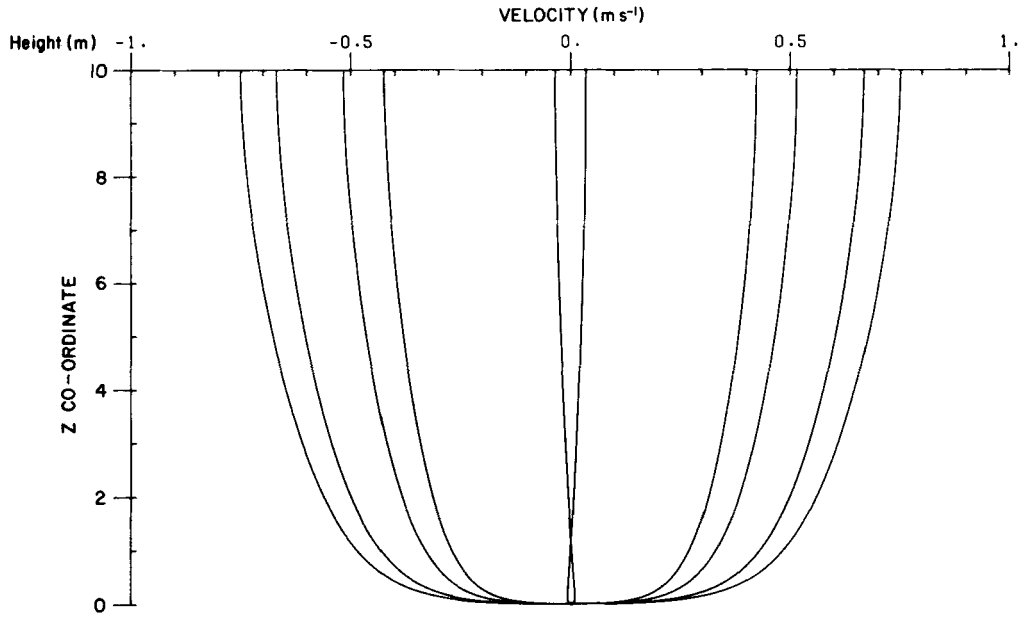
VELOCITY (m s⁻¹)
Height (m)
-1.
-0.5
0.
0.5
1.
10
8
6
4
2
0
Z CO-ORDINATE

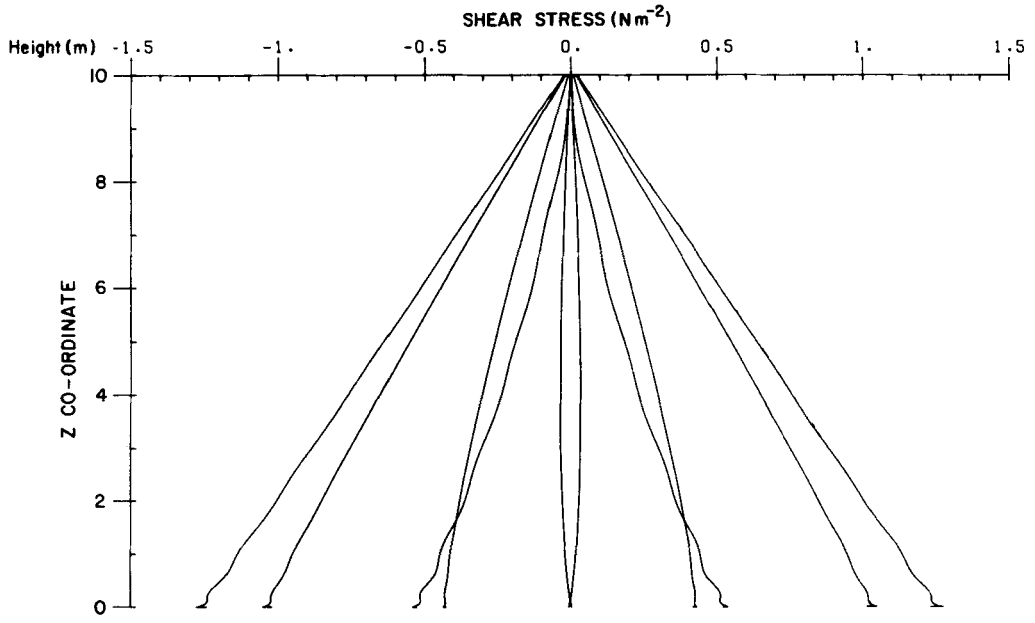
SHEAR STRESS (N m⁻²)
Height (m)
-1.5
-1.
-0.5
0.
0.5
1.
1.5
10
8
6
4
2
0
Z CO-ORDINATE

Figure 4. (a)–(b)

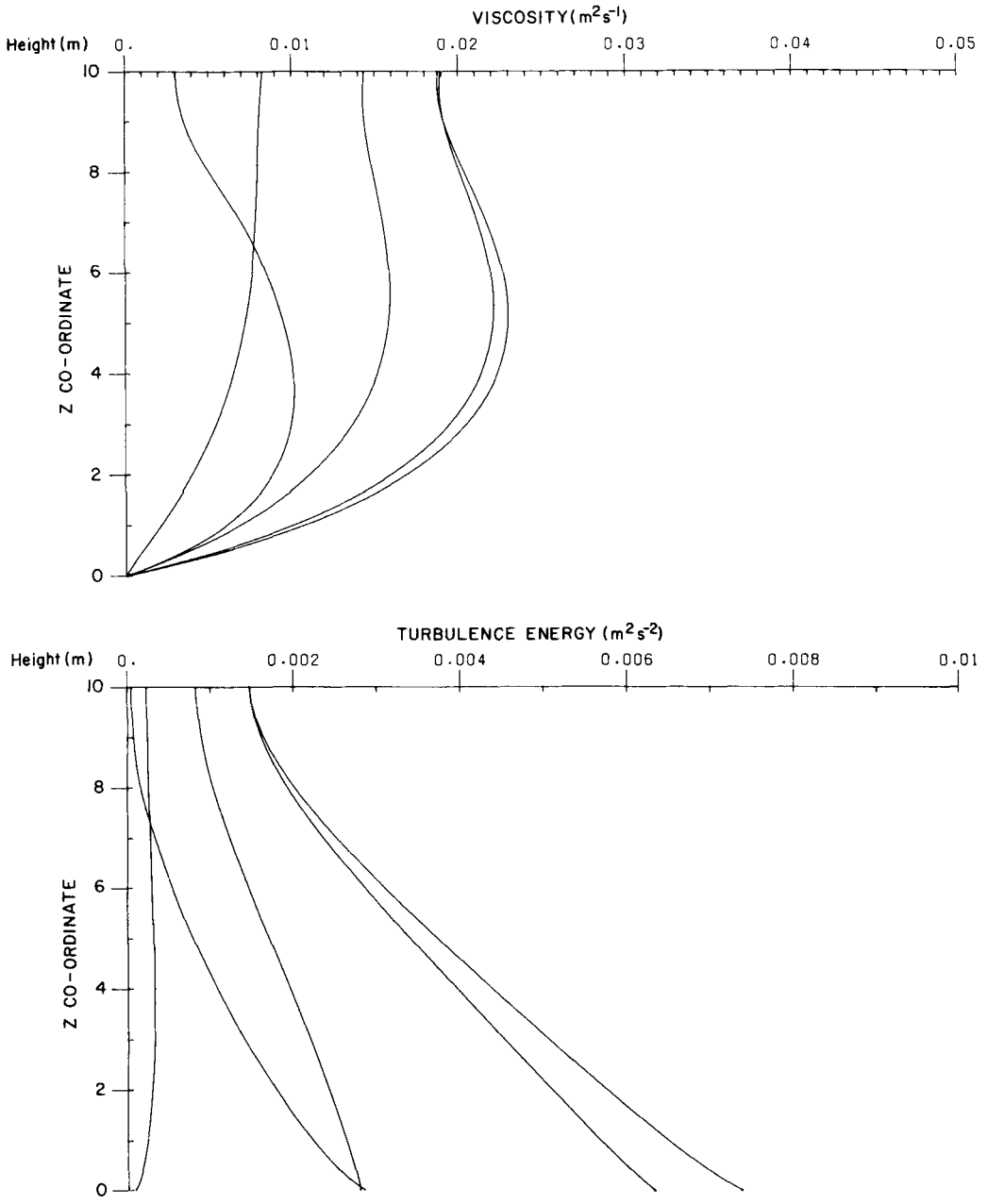

Figure 4. Profiles over an M_2 tidal period of (a) current, (b) shear stress, (c) eddy viscosity and (d) turbulence energy computed in a water depth $h = 10$ m using the mixing length formulation of Blackadar with $\gamma = 0{\cdot}4$

Figure 4(a) shows the current velocity over a tidal cycle induced by a sinusoidal oscillation of unit amplitude. It is evident from Figure 4(a) that in this case, in contrast to the wave problem, the boundary layer extends to the water surface. It is apparent that the maximum surface current is significantly less than the 1 m s^{-1} that would occur if the boundary layer thickness was less than the water depth (i.e. the wave problem). Also, for the tidal problem there is a non-zero stress (see

Figure 4(b)) through the water column, with zero stress only occurring at the surface because of the imposed boundary condition (equation (6)). (The small non-zero surface stress shown in Figure 4(b) is due to the finite difference implementation of the surface boundary condition, which gives a zero stress slightly above the water surface.)

It is evident from Figure 4(b) that the stress profile is almost linear (particularly at its maximum value) throughout the water column. However, close to the bed some small physically unrealistic oscillations are evident, and just at the bed the stress falls slightly below its maximum value. These oscillations in stress remain small provided m is of the order of 100–50. However, if m is reduced significantly below 25, large physically unrealistic oscillations can occur.

Calculations (Table IV) and plots (Figures 4(c) and 4(d)) clearly show that the viscosity and mixing length are much larger than in the wave problem, with both eddy viscosity and turbulent energy having significant values in the upper part of the water column, in marked contrast to the wave problem. A detailed discussion of the physical reasons for this is beyond the scope of this paper. However, the physical nature of this problem is sufficiently different from the previous one;

Table IV. Amplitude of M_2 tidal current and instantaneous values after 3320τ ($\tau = 372{\cdot}62$ s) computed with various grid resolutions and a range of mixing lengths. A non-staggered finite difference grid was used in the calculations and the water depth was $h = 10$ m

z(s-co-ord)	h_u(m s^{-1}) $\times 10^2$	τ(N m^{-2})	μ(m^2 s^{-1}) $\times 10^4$	b(m s^{-2}) $\times 10^2$	l(m) $\times 10^2$	Max. bed stress (N m^{-2})
$m = 100$, mixing length linearly increasing as $K(z+z_0)$ ($l = 2{\cdot}5$)						
0·01	27·41	1·025	12·81	0·478	4·00	(a) 1·304
0·25	55·86	0·801	277·4	0·367	98·93	(b) 1·315
0·75	68·34	0·283	182·3	0·154	100·20	
$m = 100$, mixing length of Vager and Kagan[8]						
0·01	27·68	1·027	12·79	0·478	3·99	(a) 1·317
0·25	57·13	0·786	258·5	0·360	92·99	(b) 1·338
0·75	65·48	0·276	522·8	0·208	247·3	
$m = 100$, mixing length of Blackadar[12] *with $\gamma = 0{\cdot}4$*						
0·01	27·03	1·024	12·56	0·627	3·91	(a) 1·245
0·25	59·46	0·804	179·1	0·482	63·62	(b) 1·271
0·75	73·68	0·286	206·7	0·213	110·50	
$m = 100$, mixing length of Blackadar[12] *with $\gamma = 0{\cdot}1$*						
0·01	24·10	0·952	11·16	0·569	3·65	(a) 0·985
0·25	66·00	0·742	79·04	0·443	29·28	(b) 0·996
0·75	97·74	0·262	59·06	0·160	36·38	
$m = 25$, mixing length of Vager and Kagan[8]						
0·01	28·89	1·099	13·09	0·517	3·93	(a) 1·472
0·25	59·16	0·845	266·3	0·381	92·93	(b) 1·472
0·75	67·89	0·330	542·9	0·224	247·5	
$m = 25$, mixing length of Blackadar[12] *with $\gamma = 0{\cdot}1$*						
0·01	24·21	0·966	11·24	0·579	3·65	(a) 1·048
0·25	66·00	0·770	81·56	0·459	29·71	(b) 1·033
0·75	98·35	0·312	65·39	0·189	37·16	

that is, it presents a further independent test of the influence of mixing length, grid differencing and time stepping upon the accuracy of the solution.

Values of the amplitude of the first harmonic, together with instantaneous values of stress, viscosity, turbulence energy and mixing length at $t = 3320\tau$ ($\tau = 372{\cdot}62$ s), a time of near-maximum surface current, are shown in Table IV for a range of mixing lengths. The majority of values presented in this table were computed using $m = 100$. Calculations showed that these results were not different (to the accuracy shown in the table) from values computed using $m = 200$ grid points, and in practice reducing m to 50 gave values which were not significantly different. However, a further reduction to $m = 25$ (see later values in Table IV) did have a noticeable affect, although in a comparison of model results with field data (where current accuracy can usually only be guaranteed to the order of 1–2 cm s^{-1}), errors in the model would probably be comparable with those in the field data.

It is evident from Table IV that currents and stresses computed using a fixed mixing length and that given by Vager and Kagan[8] are only slightly different. The eddy viscosity and turbulent energy, though similar in the near-bed region, are significantly different higher in the water column. However, in the upper part of the water column the velocity gradient is small (see Figure 4(a)) and differences in viscosity do not significantly influence the stress profile or velocity field.

The mixing length formulation of Blackadar[12] with $\gamma = 0{\cdot}4$ yields velocity and stress profiles similar to those obtained using a fixed mixing length or that given by Vager and Kagan[8] (see Table IV). However, when γ is reduced to 0·1 a significant difference can be seen (see Table IV).

A comparison of results computed using the staggered and non-staggered finite difference grids with $m = 100$ (Tables IV and V) confirmed that the solutions were independent of the grid. Also, there did not appear to be any significant advantage in using one grid compared to the other, in that both gave results of comparable accuracy with $m = 100$. When m was reduced to 25, both grids

Table V. Instantaneous values after 3320τ ($\tau = 372{\cdot}62$ s) of velocity, stress, viscosity, turbulence and mixing length for the M_2 tide in a water depth $h = 10$ m, calculated using a staggered grid in the vertical

$s = z/h$	u	τ	μ	b	l	
$m = 100$, mixing length of Vager and Kagan[8]						
0·01	22·89	0·989	13·13	0·461	4·18	(a) 1·324
0·25	47·35	0·743	258·2	0·348	95·47	(b) 1·308
0·75	54·18	0·232	510·5	0·198	250·3	
$m = 25$, mixing length of Vager and Kagan[8]						
0·01	21·94	0·937	14·67	0·439	4·79	(a) 1·271
0·25	45·69	0·677	265·6	0·335	103·1	(b) 1·265
0·75	52·19	0·141	496·6	0·185	260·1	
$m = 100$, mixing length of Blackadar[12] with $\gamma = 0{\cdot}1$						
0·01	23·13	0·933	11·52	0·560	3·80	(a) 1·019
0·25	63·23	0·717	77·57	0·438	29·21	(b) 0·993
0·75	95·60	0·220	53·95	0·153	35·96	
$m = 25$, mixing length of Blackadar[12] with $\gamma = 0{\cdot}1$						
0·01	22·72	0·904	12·69	0·547	4·24	(a) 0·987
0·25	62·70	0·668	75·10	0·434	29·27	(b) 0·980
0·75	94·56	0·144	43·20	0·155	35·29	

showed a similar loss of accuracy in the solution (compare Table V with Table IV). (It was hoped at one time that one grid might have been more accurate at low grid resolution than the other, leading to a preference for one grid over the other.) However, it is apparent from a comparison of Tables IV and V that as m is reduced from 100 to 25, the currents computed with the non-staggered grid are slightly increased whereas those computed with the staggered grid are slightly reduced. This occurs using both the mixing length formulation of Vager and Kagan[8] and that of Blackadar.[12] There does not appear to be any obvious reason for this, and the differences between solutions in Tables IV and V suggest that a value of m in excess of 25 should be used in order to obtain an accurate solution.

In these calculations the finite difference form of the dissipation term (form C) given by equations (31) and (32) was used together with the turbulence production term (41) and a time step of 372·62 s. This form of dissipation, production and time step was arrived at after a number of calculations, as shown in Table VI. In an initial series of calculations a number of different formulations of the turbulence production term were used (see Appendix). Initially finite difference form (40) was applied with $\gamma_1 = 1{\cdot}0, \gamma_2 = 0{\cdot}0$ and subsequently with $\gamma_1 = \gamma_2 = 0{\cdot}5$. In both these cases

Table VI. Bed stress and analysed amplitude of the M_2 tide in a water depth $h = 10$ m, computed using a log–linear grid with the mixing length of Vager and Kagan[8] for various forms of turbulence dissipation and time averaging

Finite difference form of dissipation	Frequency of time averaging	τ (s)	Bed stress (N m^{-2}) (a)	Bed stress (N m^{-2}) (b)	Current amplitude (m s^{-1}) $\times 10^2$ at height z above sea bed: $z = 0{\cdot}1$ m	$z = 10{\cdot}0$ m
m = 100						
A		46·58	1·263	1·291	27·34	65·21
B		46·58	1·263	1·291	27·36	65·25
C		46·58	1·266	1·294	27·38	65·30
A		93·16	∞	∞	∞	∞
B		93·16	∞	∞	∞	∞
C		93·16	1·270	1·300	27·39	65·48
C		186·31	1·288	1·312	27·48	65·74
C		372·62	1·317	1·338	27·68	66·29
C		558·93	1·347	1·367	27·98	67·14
C		745·24	1·389	1·394	28·22	67·78
C		1490·48	1·490 *	1·470 *	29·27	70·42
m = 25 with time averaging						
A, B	10	93·16	1·411	1·421	28·59	68·12
A, B	10	372·62	1·460 *	1·446 *	28.76	68·60
A, B	10	558·93	2·317 *	1·598 *	28·82	68·79
A, B	3	93·16	1·409	1·420	28·61	68·15
A, B	3	372·62	1·507 *	1·490 *	28·72	68·50
A, B	3	558·93	1·586 *	1·729 *	28·66	68·52
A, B	3	745·24	2·607 *	1·470 *	29·34	69·34

∞ Indicates values exceeded physically realistic values.
* Indicates existence of time step oscillations.

large time step oscillations occurred in the computed bed stress even with the time step τ reduced to 93·16 s. Subsequently the form of turbulence production given by equation (41) with $\gamma_1 = \gamma_2 = 0{\cdot}5$ was used together with formulation C for the turbulence dissipation. This gave solutions which with time steps up to 745 s did not exhibit time step oscillations in the computed bed stress. The reason for the enhanced stability of the finite difference form (41) is not clear. It is evident from (41) that by linearly combining the shear at time $t+\tau$ with that at t, with $\gamma_1 = \gamma_2 = 0{\cdot}5$, then any time step wave will be removed before the shear is squared. Such a time step wave would not, however, be removed by (40), since the shear is squared before being averaged in time. This difference may be part of the reason why difference scheme (41) is more stable.

Table VI shows values of maximum bed stress computed using equations (15) (column (a)) and (16) (column (b)), together with the amplitude of the M_2 harmonic of the current at heights of 0.1, 1 and 10 m (free surface) above the bed. The various finite difference forms (A, B and C) of the dissipation term were used in these calculations, together with a range of time steps.

Initially no form of iteration or time smoothing was applied. Under these conditions calculations showed that the finite difference forms A and B of the dissipation term were only stable with time steps of order 46 s (without iteration or time filtering) and that the solution with this time step was essentially independent of the finite difference form of the dissipation term (Table VI). At larger time steps only dissipation form C was stable; however, at time steps of the order of 1490 s (approximately 24 min) the error in the solution was unacceptably large owing to time discretization errors. (This is to be anticipated, since one would not expect to accurately reproduce a wave period of the order of 12 h with a time step of order 0·5 h.) However, it is interesting to note that dissipation form C remained stable at these large time steps and that with a time step of order 372 s gave an accurate solution. (In a large-scale three-dimensional model a time step of order 10 min would appear appropriate, giving rise to an inaccuracy in surface current only of the order of 2 cm s^{-1} and 5° in phase.)

These calculations were performed using 100 grid points in the vertical. With reduced resolution ($m = 25$) (Table VI) dissipation forms A and B yielded stable solutions with time steps up to 745·24 s provided some time filtering was included (Table VI). In practice this time filtering was included using the Schuman[14] filter, since this avoided the computational overhead of having to compute the $\bar{F}(t-\tau)$ term in the Asselin[15] filter. It is evident from Table VI that with $m = 25$, $\tau = 372{\cdot}62$ s and time averaging every third or 10th time step, numerical stability could be enhanced with dissipation forms A and B, although some oscillations in the bed stress were still present. However, it is evident from Tables V and VI that the maximum bed stress obtained with $m = 25$ is physically unrealistically high and may be unacceptable in some applications.

The dissipation forms A and B could also be used with longer time steps provided some iteration was performed on the viscosity and mixing length. However, the computational time was similar, as one would expect, to that obtained by reducing the time step.

In order to appreciate in some detail the origin of the instabilities which occur with dissipation forms A or B, it is instructive to examine the time series of current and bed stress prior to the instabilities corrupting the solution. Figures 5(a) and 5(b) show time series of currents at various depths (a depth of 0·01 m corresponding to a height of eight grid points from the sea bed) and modulus of bed stress computed with dissipation form A and a time step of 258·76 s. A water depth $h = 10$ m, the mixing length of Blackadar[12] with $\gamma = 0{\cdot}4$, and 100 grid points were used in the calculation. The time series shown here was obtained approximately two tidal cycles before the solution was corrupted by instabilities. Values were plotted at each time step and no filtering or time smoothing was applied.

It is evident from Figure 5(a) that there is a significant time step oscillation in the near-bed current, and evidence of this was found higher in the water column. The modulus of bed stress

computed from (15) showed severe time step oscillations (see Figure 5(b)), which eventually corrupted the solution. An instantaneous profile of the stress also showed significant grid point oscillations through the vertical, having maximum oscillations close to the bed. In contrast, Figure 5(c) shows the bed stress after many tens of tidal cycles, for the same problem but with turbulence dissipation C.

These calculations clearly identified the finite difference forms of the turbulence production and dissipation terms as being crucial in determining the stability of the solution.

In a final series of calculations, rotational effects were included, with $f = 0{\cdot}00012\ s^{-1}$, typical of the North Sea. As would be expected, the influence of rotation did not affect the stability of the solution or its accuracy.

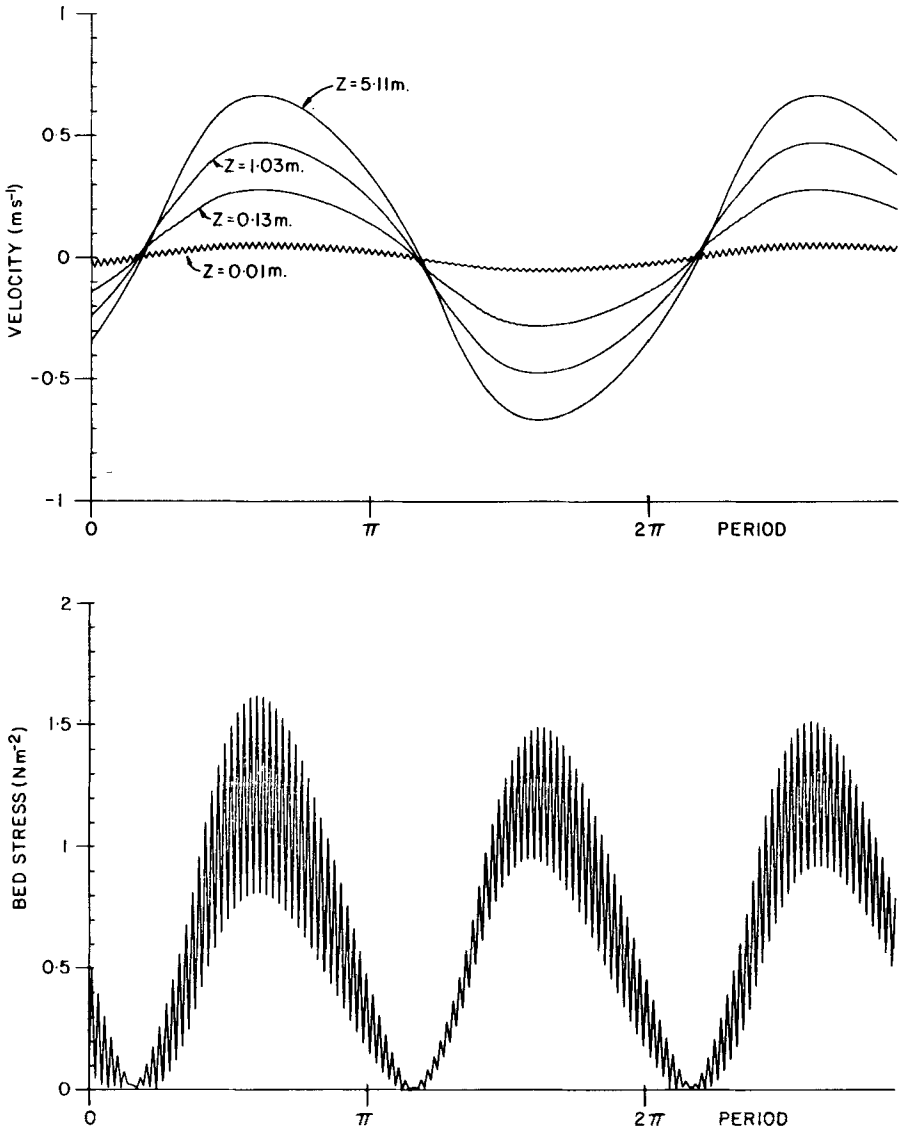

Figure 5. (a)–(b)

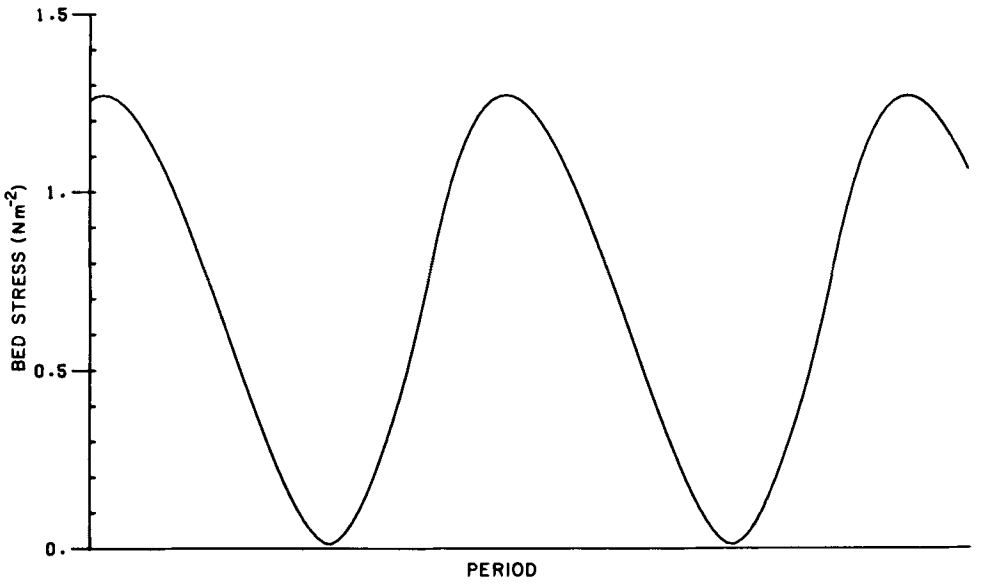

Figure 5. Time series of (a) tidal currents at four depths, (b) modulus of bed stress computed with turbulence dissipation form A and (c) modulus of bed stress computed with turbulence dissipation form C. Calculations are for an M_2 tide in a water depth $h = 10$ m using Blackadar's mixing length with $\gamma = 0{\cdot}4$

4.3. Tidally induced flow, water depth $h = 100$ m, wave of M_2 tidal period ($T = 12{\cdot}42$ h)

In the previous series of calculations the water depth h was taken as $h = 10$ m, typical of a near-coastal region. However, in a large-area continental shelf model, water depths ranging between 10 m and several hundred metres will occur. To test the stability and accuracy of the various finite difference methods, and the influence of mixing length formulation upon the solution, a final series of calculations were performed for a rectilinear tidal flow induced by unit forcing in a water depth of 100 m.

Values of amplitude of the first harmonic, together with instantaneous values of velocity, stress, viscosity, turbulence energy and mixing length at $t = 3320\tau$ ($\tau = 372{\cdot}62$ s), a time of near-maximum surface current, are shown in Table VII. Various formulations of the mixing length were used in these calculations, together with a number of values of m, both on logarithmic and log–linear transformed co-ordinates.

Calculations showed that even in a depth of 100 m, the tidal current only reached its free stream value close to the sea surface and that a non-zero stress occurred below the surface layer.

Values of eddy viscosity and mixing length were found to be significantly larger (see Table VII) in the near-surface region in this example than in the case of a water depth of 10 m. Consequently this calculation provides a further test of the accuracy of the various difference schemes in a highly viscous flow regime (see viscosity values in Table VII).

Calculations using the various mixing lengths presented in Section 2, with the turbulence energy dissipation form C, with $m = 100$ and $\tau = 372{\cdot}62$ s are presented in Table VII, together with some results computed with $m = 200$. In all cases the calculations remained stable, and no significant increase in accuracy was obtained when m was increased from 100 to 200 grid points (see

Table VII. Amplitude of M_2 tidal current and instantaneous values after 3320τ ($\tau = 372{\cdot}62$ s) computed with various grid resolutions and a range of mixing lengths in a water depth $h = 100$ m

s-co-ord.	$h(\mathrm{m\,s^{-1}}) \times 10^2$	$\tau(\mathrm{N\,m^{-2}})$	$\mu(\mathrm{m^2\,s^{-1}}) \times 10^4$	$b(\mathrm{m\,s^{-2}}) \times 10^2$	$l(\mathrm{m}) \times 10^2$	Max. bed stress ($\mathrm{N\,m^{-2}}$)
$m = 100$, mixing length linearly increasing as $K(z+z_0)$ ($l = 25$)						
0·001	34·18	1·868	16·83	0·825	4·00	(a) 2·034
0·1	85·68	1·438	1411·0	0·580	400·0	(b) 2·038
0·25	94·55	0·940	2739·0	0·350	1000·0	
$m = 100$, mixing length of Vager and Kagan[8]						
0·001	34·10	1·768	16·44	0·795	3·98	(a) 1·972
0·1	86·14	1·388	1297·0	0·573	369·9	(b) 2·011
0·25	95·96	0·931	2240·0	0·349	818·4	
$m = 100$, log–linear grid, mixing length of Blackadar[12] *with $\gamma = 0{\cdot}4$*						
0·001	32·25	1·681	15·92	0·969	3·99	(a) 1·779
0·1	83·14	1·196	1017·0	0·640	313·6	(b) 1·783
0·25	94·37	0·637	1358·0	0·320	592·2	
$m = 200$, logarithmic grid, mixing length of Blackadar[12] *with $\gamma = 0{\cdot}4$*						
0·001	32·17	1·681	15·91	0·968	3·99	(a) 1·791
0·1	83·09	1·200	1018·0	0·641	313·6	(b) 1·774
0·25	94·32	0·638	1361·0	0·321	592·3	
$m = 100$, log–linear grid, mixing length of Blackadar[12] *with $\gamma = 0{\cdot}1$*						
0·001	29·00	1·412	14·54	0·826	3·95	(a) 1·423
0·1	82·55	0·812	463·6	0·460	168·6	(b) 1·426
0·25	99·58	0·153	270·5	0·087	225·7	
$m = 200$, logarithmic grid, mixing length of Blackadar[12] *with $\gamma = 0{\cdot}1$*						
0·001	28·95	1·412	14·54	0·825	3·95	(a) 1·438
0·1	82·52	0·814	464·2	0·461	168·6	(b) 1·420
0·25	99·56	0·156	272·5	0·088	225·8	

Table VII) and the transformation changed from log–linear to logarithmic in order to enhance near-bed resolution.

It is evident from Table VII that the eddy viscosity increases rapidly with height above the bed in the cases of a linearly increasing mixing length and that of Vager and Kagan.[8] A similar increase occurs with the mixing length of Blackadar[12] when $\gamma = 0{\cdot}4$, although when $\gamma = 0{\cdot}1$ an increase and subsequent decrease occur (Table VII). It is evident from Table VII that the maximum bed stress computed with $\gamma = 0{\cdot}1$ is significantly lower than with the other mixing lengths. To test that this was physically realistic and as a further check on the accuracy of the solution, the calculations using $\gamma = 0{\cdot}4$ and $0{\cdot}1$ were repeated with the logarithmic transformation (which gave maximum near-bed resolution) with $m = 200$. It is evident from Table VII that this gave no significant change in the accuracy of the results.

These calculations show that there are significant differences in the magnitude of the eddy viscosity in shallow and deep water, and that its magnitude does depend upon the mixing length formulation. A highly accurate solution can be obtained with $m = 100$, and solutions of acceptable accuracy with m of order 25–50.

5. CONCLUDING REMARKS

In this paper we have investigated the accuracy and stability of a number of finite difference schemes for the solution of the turbulence energy equations describing wave and tidally induced motion. The primary aim here has been to develop a stable, accurate and computationally efficient method that can be used in the three-dimensional simulation of tides in large sea areas such as continental shelves.[11] The numerical schemes developed here will also be useful in more limited area simulations of the interaction of waves and currents.

Calculations have shown that accurate solutions can be obtained using staggered or non-staggered finite difference grids in the vertical, with the order of 50 grid points from sea bed to sea surface. The transformation of the equations onto a logarithmic or log–linear co-ordinate scale in the vertical is particularly important to ensure a high grid resolution in the near-bed region, where large vertical shears occur. The choice of staggered or non-staggered grid may be computationally important for certain computer architectures.

Time discretization has been accomplished using the Crank–Nicolson method, giving a semi-implicit time-stepping algorithm. Although this method is unconditionally stable when used to integrate a diffusion equation, calculations showed that the stability of the numerical solution of the set of coupled hydrodynamic and turbulence energy equations depended upon the time discretization of the production and dissipation terms in the turbulence energy equation.

Although it was not the intention in this paper to investigate the influence of mixing length on the solution (but rather to check that the difference scheme was accurate for a range of mixing lengths), it is interesting to note its influence upon the solution—a topic which merits further calculations under a range of z_0-values.

The finite difference scheme developed in this paper, with turbulence energy dissipation form C, is presently being used in a series of wave–current interaction problems and in a large-scale three-dimensional tidal simulation.[11] Results of these calculations will be reported in due course.

ACKNOWLEDGEMENTS

The authors are indebted to Dr. B. M. Jamart and J. Ozer for a number of valuable discussions during the course of this work. The care and effort taken by Mrs. J. Huxley in typing the text and Mr. R. A. Smith in preparing the diagrams is appreciated. The work was funded in part by the Procurement Executive, Ministry of Defence.

APPENDIX

Here we briefly consider two difference forms of the term

$$\left[\left(\frac{\partial u}{\partial \sigma}\right)^2+\left(\frac{\partial v}{\partial \sigma}\right)^2\right], \tag{39}$$

which occurs in equation (25) and represents the generation of turbulent kinetic energy.

Defining two coefficients γ_1 and $\gamma_2=1-\gamma_1$ such that $0\leqslant\gamma_1\leqslant 1$ (see Section 3), (39) can be determined at any time over a time step τ from

$$[\gamma_1(\delta U_{k-1}^{t+\tau})^2+\gamma_2(\delta U_{k-1}^{t})^2]+[\gamma_1(\delta V_{k-1}^{t+\tau})^2+\gamma_2(\delta V_{k-1}^{t})^2], \tag{40}$$

with δ a vertical difference operator (see Section 3).

An alternative to (40), which will be shown to have enhanced numerical stability and yield answers of similar accuracy, is given by

$$(\gamma_1 \delta U_{k-1}^{t+\tau} + \gamma_2 \delta U_{k-1}^{t})^2 + (\gamma_1 \delta V_{k-1}^{t+\tau} + \gamma_2 \delta V_{k-1}^{t})^2. \tag{41}$$

For the case in which $\gamma_1 = \gamma_2 = 0{\cdot}5$, the turbulence production term is centred with respect to the time step τ. With this choice of γ_1 and γ_2 it is evident that the difference form (41), by time averaging before squaring, will remove any time step oscillation in the production term, whereas (40), by squaring before time averaging, does not remove such an oscillation. This is probably the major reason why the difference scheme (41) was found preferable to (40) and was used in the calculations.

The choice of difference scheme (40) or (41) is related to the ability of various difference schemes to conserve physical properties and is discussed by Lee *et al.*[18]

REFERENCES

1. A. G. Davies, 'A numerical model of the wave boundary layer', *Continental Shelf Res.*, **6,** 715–739 (1986).
2. H. L. King, A. G. Davies and R. L. Soulsby, 'A numerical model of the turbulent boundary layer beneath surface waves and tides', *Institute of Oceanographic Sciences, Report No. 196*, 1985.
3. A. G. Davies, R. L. Soulsby and H. L. King, 'A numerical model of the combined wave and current bottom boundary layer', *J. Geophys. Res. (Oceans)*, **93,** 491–508 (1988).
4. T. J. Smith, 'On the representation of Reynolds stress in estuaries and shallow coastal seas', *J. Phys. Oceanogr.*, **12,** 914–921 (1982).
5. K. F. Bowden and S. R. Ferguson, 'Variations with height of the turbulence in a tidally-induced bottom boundary layer', in J. C. J. Nihoul (ed.), *Marine Turbulence; Proc. 11th Liege Colloq. on Ocean Hydrodynamics*, Elsevier, Amsterdam, 1979, pp. 259–286.
6. A. M. Davies, 'A three-dimensional model of the Northwest European Continental Shelf, with application to the M_4 tide', *J. Phys. Oceanogr.*, **16,** 797–813 (1986).
7. A. M. Davies and G. K. Furnes, 'Observed and computed M_2 tidal currents in the North Sea', *J. Phys. Oceanogr.*, **10,** 237–257 (1980).
8. B. G. Vager and B. A. Kagan, 'The dynamics of the turbulent boundary layer in a tidal current', *Atmos. Oceanic Phys.*, **5,** 168–179 (1969).
9. H. O. Mofjeld and J. W. Lavelle, 'Setting the length scale in a second-order closure model of the unstratified bottom boundary layer', *J. Phys. Oceanogr.*, **14,** 833–839 (1984).
10. B. Johns, 'The modelling of tidal flow in a channel using a turbulence energy closure scheme', *J. Phys. Oceanogr.*, **8,** 1042–1049 (1978).
11. A. M. Davies and J. E. Jones, 'Application of a three dimensional turbulence energy model to the determination of tidal currents on the Northwest European Continental shelf', to appear in *J. Geophys. Res. (Oceans)*.
12. A. K. Blackadar, 'The vertical distribution of wind and turbulent exchange in a neutral atmosphere', *J. Geophys. Res.*, **67,** 3095–3120 (1962).
13. J. Noye, *Numerical Simulation of Fluid Motion*, North-Holland, Amsterdam, 1978.
14. F. G. Schuman, 'Numerical methods in weather prediction: II—Smoothing and filtering', *Mon. Weather Rev.*, **85,** 357–361 (1957).
15. R. Asselin, 'Frequency filtering for time integrations', *Mon. Weather Rev.*, **100,** 487–490 (1972).
16. R. Shapiro, 'Smoothing, filtering and boundary effects', *Rev. Geophys. Space Phys.*, **8,** 359–388 (1970).
17. A. M. Davies and J. E. Jones, 'Modelling turbulence in shallow sea regions', in J. C. J. Nihoul and B. M. Jamart (eds), *Small-scale Turbulence and Mixing in the Ocean*, Oceanographic Series, Elsevier, Amsterdam, 1988, pp. 63–76.
18. R. L. Lee, P. M. Gresho, S. T. Chan and R. L. Sani, 'A comparison of several conservation forms for finite-element formulations of incompressible Navier–Stokes or Boussinesq equations', *Proc. Third Int. Conf. on Finite Elements in Flow Problems*, Banff, Canada, 1980, pp. 216–227.